# 7 CURE CHARACTERISATION: DIELECTRIC SPECTROSCOPY

This chapter focuses on the results of the dielectric spectroscopy carried out isothermally on several of the systems. The real and imaginary permittivity were followed as a function of time and frequency, by performing frequency scans from 1Hz to 1MHz at set time intervals. The results were then compared to those from the previous results chapters.

## *7.1 INTRODUCTION*

As in previous chapters the dielectric properties will be discussed for each system separately, however it is appropriate to make some general comments to avoid subsequent repetition.

The dielectric permittivity (ε'(ω)) and dielectric loss (ε"(ω)) change as a function of both frequency and time and may be presented in 3D plots. Example 3D plots for the Strathclyde Model system cured at 25°C, for the real and imaginary permittivity, are shown in Figure 1 and Figure 2. An alternative format is to present the data in the form of a 2D plot (Figure 3 and Figure 4). This presentation helps to visualise the way in which the dielectric relaxation features change with the cure time and will be used for the presentation of the data on all of the systems investigated. The techniques used in the previous chapters follow changes in the system within a fixed frequency and rate window and later in this chapter the variation of the dielectric properties as observed at a frequency of 2Hz with cure time will be presented. This latter data allow closer comparison between the observations made using the curemeter and Differential Scanning Calorimetry measurements.

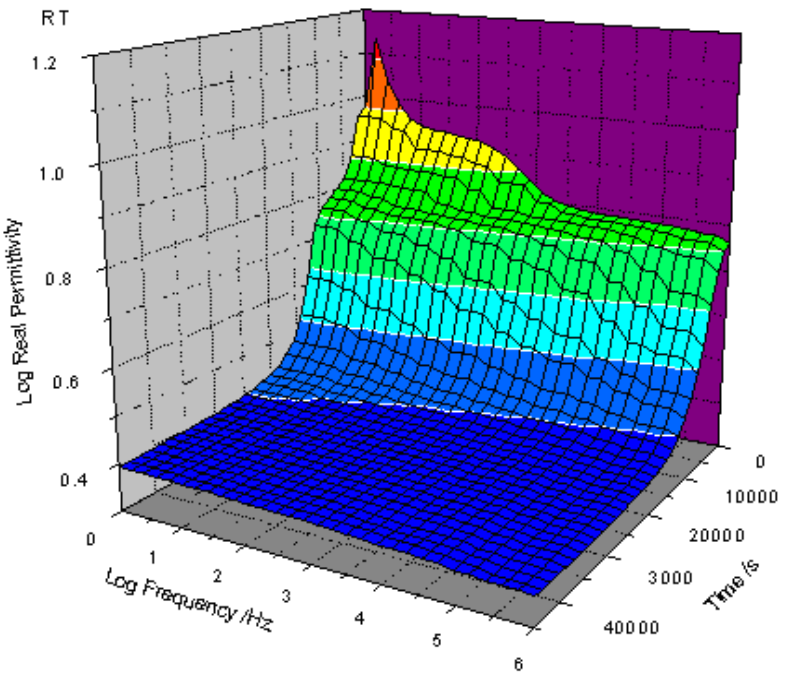


**Figure 1. 3D plot of the variation of the changes in the real permittivity as a function of frequency and cure time for Strathclyde model system cured at 25°C.**

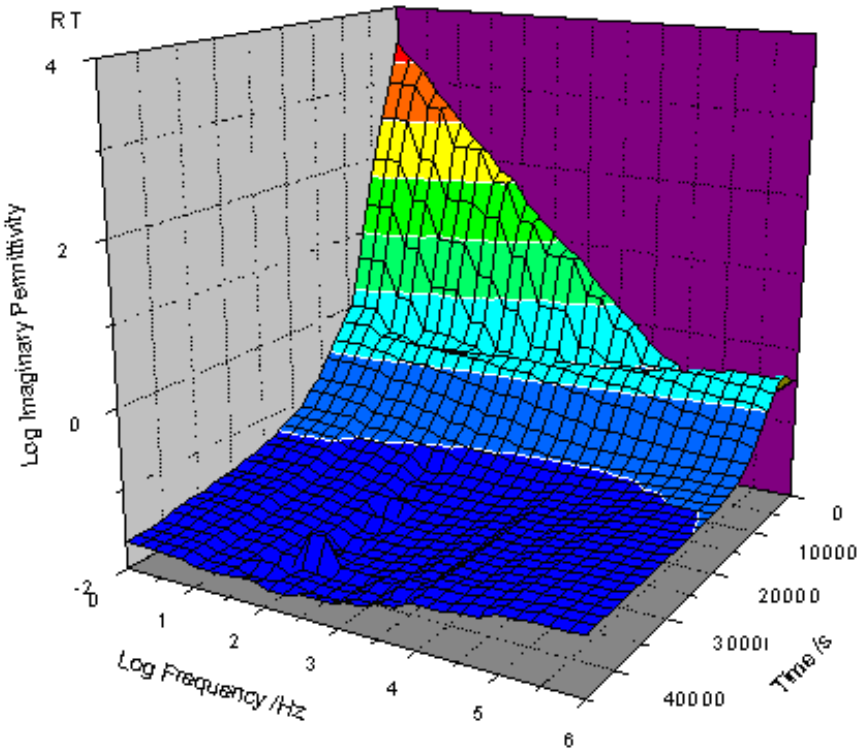


**Figure 2. 3D plot of the variation of the changes in the imaginary permittivity as a function of frequency and cure time for Strathclyde model system cured at 25°C.**

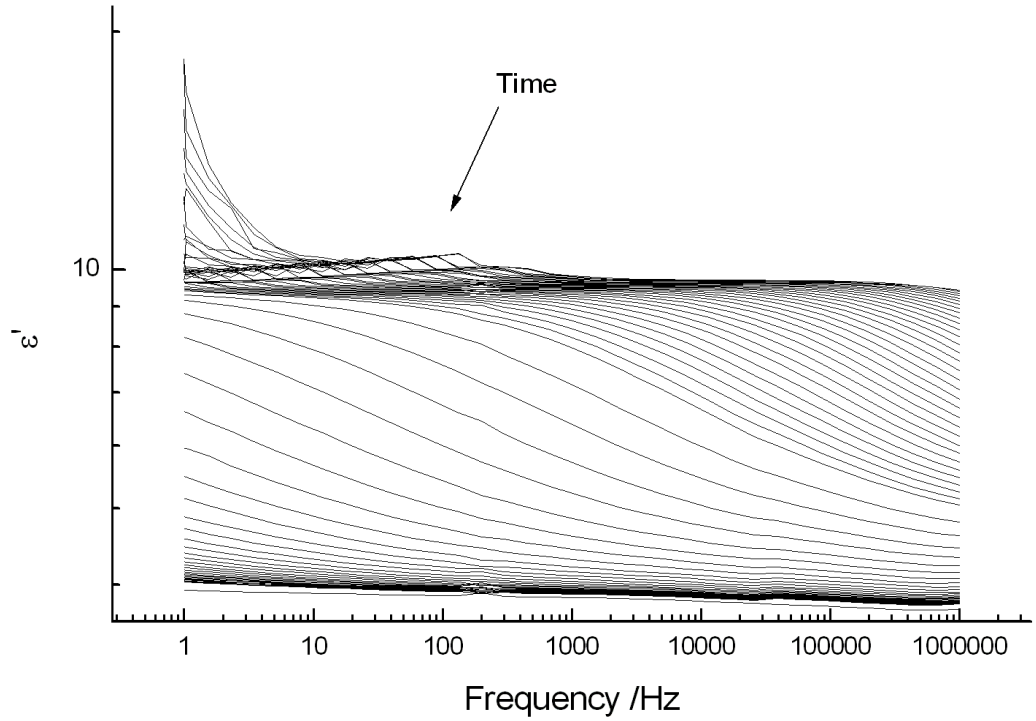


**Figure 3. 2D plot of real permittivity for the Strathclyde model system cured at 25°C as a function of cure time.**

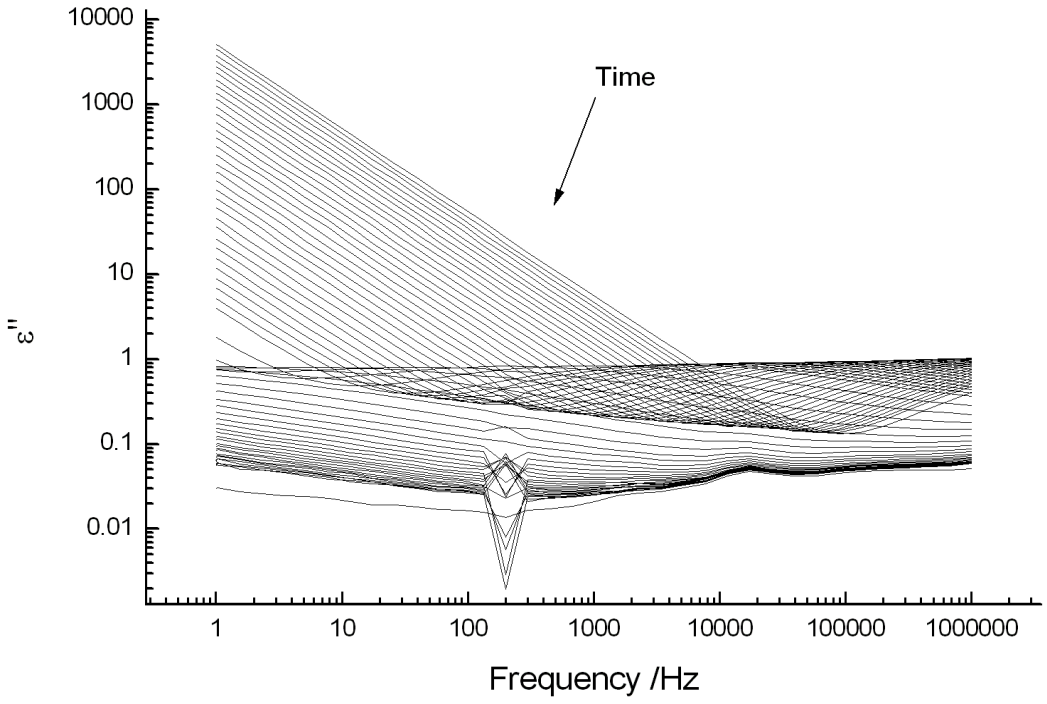


**Figure 4. 2D plot of imaginary permittivity for the Strathclyde model system cured at 25°C as a function of cure time.**

The dielectric permittivity reflects the ability to induce polarisation in a material when an external field is applied and is sensitive to all processes which are associated with changes in charge distribution, i.e. ionic migration and dipolar reorientation. The negative anomaly in the imaginary permittivity (ε”(ω)), in both Figure 2 and Figure 4, is an instrumental artefact arising from mains interference being detected by the network analyser. The interference influences the phase measurement but does not have any influence on the capacitance measurement, i.e. values of ε’(ω).

The initial dielectric spectrum is characteristic of a low molecular weight liquid in which the dipoles are able to freely rotate - this is reflected in a relatively high value of the real permittivity and has a value of approximately 6 for the Strathclyde model system, identified by the plateau value which at intermediate times gives a constant value from 1Hz to ~ 100,000Hz. Initially there is an additional contribution to the values of ε’(ω) at lower frequencies which can be attributed to processes associated with ionic mobility in the system. Ionic contamination is typically found in epoxy resins as a consequence of the use of epichlorohydrine in the synthesis of the monomer. The chloride ions, in the presence of an external field, will migrate towards the positive electrode and give rise to electrical conduction. If within the liquid this conduction process is inhibited, either by blocking electrodes or heterogeneity, then a contribution to the dielectric permittivity can be observed and is clearly identifiable in Figure 1 and Figure 3. As the cure proceeds the viscosity of the liquid will increase slowing down the rate at which the ionic impurities can move through fluid and as a consequence the amplitude of this low frequency feature is reduced and because it is slowed down it moves to lower frequency – clearly indicated in Figure 3. The initial ε”(ω) plots, Figure 2 and Figure 4, are dominated by the motion of the ionic impurities giving a direct current conductivity contribution to the dielectric loss. The dc conductivity contribution is characterised by a dependence of ε”(ω) which decreases linearly with increasing ω.

The frequency dependence of the real and imaginary dielectric responses can be represented by Equations 2.32 and 2.33 given in *Chapter 2*. A more complete description of the behaviour would be:

$$\varepsilon'(\omega) = \bar{\varepsilon}_\infty + \frac{\bar{\varepsilon}_1 - \bar{\varepsilon}_2}{1+\omega^2\tau_{MW}^2} + \frac{\bar{\varepsilon}_2 - \bar{\varepsilon}_\infty}{1+\omega^2\tau_{dipole}^2}$$

**Equation 7.1**

and

$$\varepsilon''(\omega) = \bar{\varepsilon}_\infty + \frac{\left(\bar{\varepsilon}_1 - \bar{\varepsilon}_2\right)\omega\tau_{MW}}{1+\omega^2\tau_{MW}^2} + \frac{(\bar{\varepsilon}_2 - \bar{\varepsilon}_\infty)}{1+\omega^2\tau_{dipole}^2} + \frac{\bar{\sigma}}{\omega}$$

**Equation 7.2**

where $\varepsilon_1$ is the lowest frequency value of the real permittivity, $\varepsilon_2$ is the intermediate value of the real permittivity and reflects the limiting low frequency value for the dipole relaxation and $\varepsilon_\infty$ is the high frequency limiting value of the permittivity associated with atomic polarisation and electronic polarisation of the material. The relaxation times for the ionic conduction process, designated $\tau_{MW}$ and the dipolar processes designated $\tau_{dipole}$ are clearly very different. The $\tau_{MW}$ response is initially located at a frequency of ~100Hz, whereas the $\tau_{dipole}$ is relaxing at a frequency above 1MHz.

As the cure proceeds the viscosity of the system increases and as a consequence it becomes more difficult for ionic migration to occur resulting in a slowing down of $\tau_{MW}$ response which eventually has lost both amplitude and disappears below the range of measurement. The $\tau_{dipole}$ process is also observed to slow down and move through the window of observation and is most clearly seen in Figure 3. At the end of the cure process dipole relaxation will have ceased and a glass created – vitrification has occurred.

The gelation process will effectively stop long range migration of ionic impurities and is marked by the disappearance of the dc contribution to Equation 7.2 and is easily identified by the loss of the $1/\omega$ contribution in Figure 4. The point at which it

disappears depends upon the frequency of observation and reflects the growing size of the gel structure inhibiting motion of the ions – the point at which it disappears from the window of measurement is an indication of gelation occurring in the material.

The residual loss features in the cured material can be associated with the restricted dipolar motion of pendant OH groups created during the cure process by the opening of the epoxy ring and are associated with a β type of process once the material has passed through its $T_g$.

Due to the viscous nature and difficulty of achieving a representative sample of SK31 and SP340 these were not analysed by dielectric spectroscopy. It was felt that the only way to introduce the material into the 2mm gap in the cell would be to trowel it in. As this would take a reasonable amount of time to do while trying to avoid introducing air into the de-gassed samples, it was felt too many errors may be introduced. All of the other systems were studied at several isothermal temperatures to allow a comparison with the previous results. No repeat measurements were made for any of the samples.

## *7.2 STRATHCLYDE MODEL SYSTEM*

Figure 3 and Figure 4 above show the changes in permittivity, plotted against frequency, as a function of cure time for the Strathclyde model system at 25°C. Plots for the samples held isothermally at room temperature (ca. 30°C in the instrument at the time of the work being carried out), 30°C, 40°C and 50°C can be found in the Appendix B (Figures 29-36), and show the same trends. It is however noticeable that increasing the temperature to 40°C removes the ionic contribution to the real part of the dielectric permittivity and the loss contribution will therefore be purely due to ionic conduction, the effects of heterogeneity having now disappeared and the relaxation being just a function of dipolar relaxation and ionic conduction. Increasing the temperature decreases the time for the changes in the dielectric

spectrum to occur and reflects the changes in physical properties observed with the other techniques.

To carry out a comparison of the dielectric data with viscosity and DSC data, the dielectric data obtained at 2Hz for the isothermal cure of the Strathclyde model system were plotted against time and shown in Figure 5 and Figure 6.

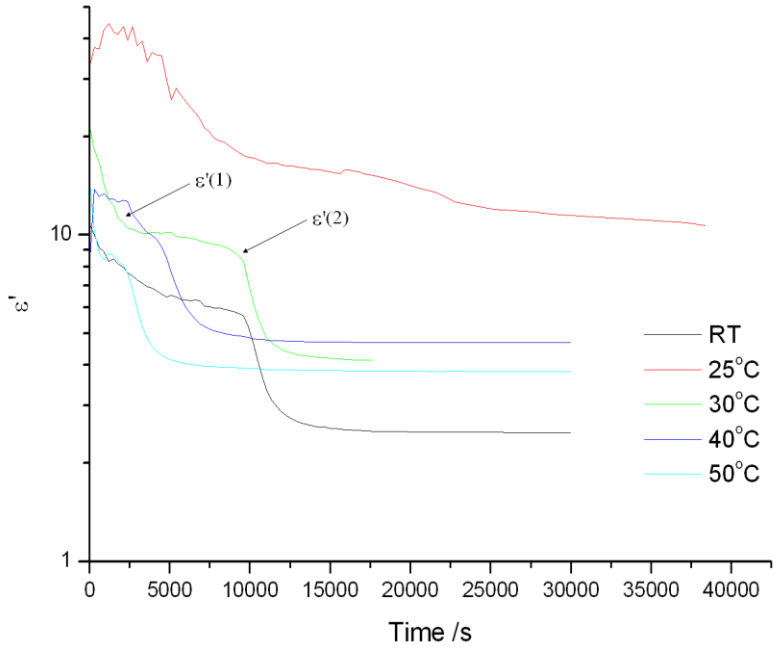


**Figure 5. Plot showing change in real permittivity at 2Hz throughout cure as a function of cure temperature for Strathclyde model system.**

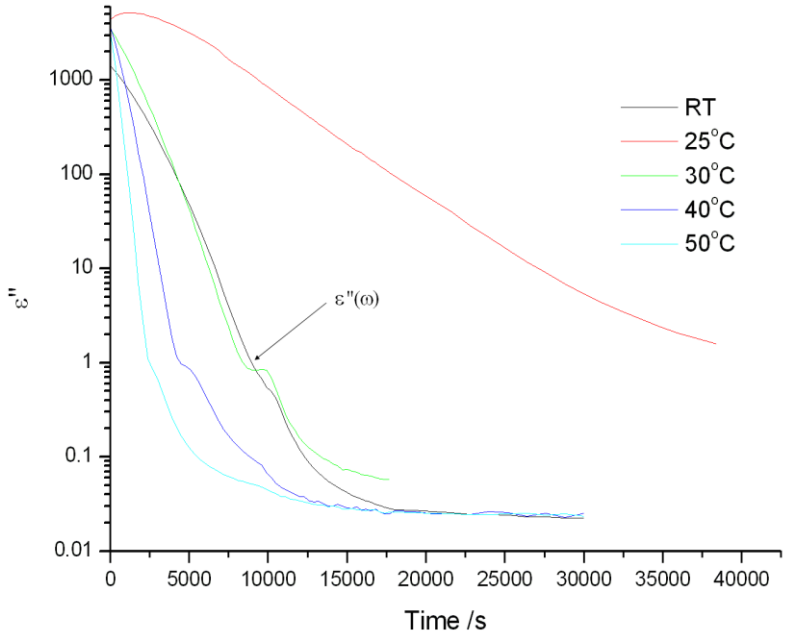


**Figure 6. Plot showing change in imaginary permittivity at 2Hz throughout cure as a function of cure temperature for Strathclyde model system.**

A step drop in the values of ε', clearly be seen in Figure 5 (indicated for 30°C trace), corresponds to the loss of the dipole relaxation as the system is transformed from a gel to a glass phase. This change is less distinct in the 25°C plot and the residual value of the real permittivity is high indicating that there still exists in the material a significant degree of dipolar activity. The low degree of cure and high dipolar activity is consistent with a low degree of conversion during polymerisation and a significant level of unreacted monomer remaining in the system. The ionic conductivity as reflected in the ε" plot (Figure 6) similarly has a high value at the end of the cure process reflecting a high level of ionic mobility and the material being still in a rubbery state.

Measurements of ε" at the higher temperatures show a much lower level being achieved which is consistent with the total loss of the dc conductivity contribution and the material being transformed to the glassy state consistent with completion of the cure process. Different levels of the residual ε' reflect varying amounts of unreacted monomer retained in the vitreous state and also varying amounts of OH creation as a consequence of the cure process.

Inspection of the dielectric data allows certain critical points in the plots to be identified:-

- the point at which gelation occurs as indicated by the loss of the $1/\omega$ dependence which appears as a change in slope in the ε" versus time plot, annotated on Figure 6 as ε"(ω).
- the point at which vitrification occurs as indicated by the cessation of dipole activity, annotated on Figure 5 as ε'(2), and is associated with the $T_g$.
- ε'(1) (Figure 5) denotes the position at which the contribution from heterogeneity, blocking electrode effects and phase separation ceases to contribute to the dielectric permittivity and will occur around the time at which gelation occurs.

Analysis of the data provides an estimate of the turning points, given as time in seconds, as indicated in Table 1.

**Table 1. Turning points for the Strathclyde model system (times in seconds).**

| Cure Temperature /°C | ε'(1) /s | ε'(2) /s | ε" /s |
|---|---|---|---|
| 25 | 16000 | 22000 | >40000 |
| RT | 2500 | 10000 | 11000 |
| 30 | 3000 | 10800 | 8000 |
| 40 | 2500 | 5000 | 5000 |
| 45 | 1500 | 2500 | 2500 |

As indicated above the point at which the conduction contribution to ε"(ω) disappears can be related to the immobilisation of ions in the matrix. It is clear that at 25°C even at the end of the cure process there is a significant contribution from ionic conduction and the matrix is in a gel state. Inspection of ε' allows identification of ε'(1) as a point where the matrix has become homogeneous and supports the idea that gelation has occurred, however the cessation of dipolar activity associated with the $T_g$ process is not identified. Increasing the cure temperature allows a more precise identification of the turning points. In general the drop in ε' associated with creation of a homogeneous matrix appears to occur before the

cessation of conduction identified by ε". This implies that the loss of the Maxwell Wagner Sillers contribution is a precursor of gelation rather than an indication that it has occurred. As the temperature is increased the time at which gelation is detected in ε" and in ε' comes closer together.

The activation energy, for each of the points of interest, was calculated as discussed in previous chapters from the Arrhenius plots (Figure 7). The lower temperatures were removed from the plot as it was believed that these were below the operating temperature of the instrument. The values were:

$$\mathbf{E_a\ (\varepsilon") = 58.3\ kJ\ mol^{-1}}$$

$$\mathbf{E_a\ (\varepsilon'(1)) = 33.5\ kJ\ mol^{-1}}$$

$$\mathbf{E_a\ (\varepsilon'(2)) = 75.5\ kJ\ mol^{-1}}$$

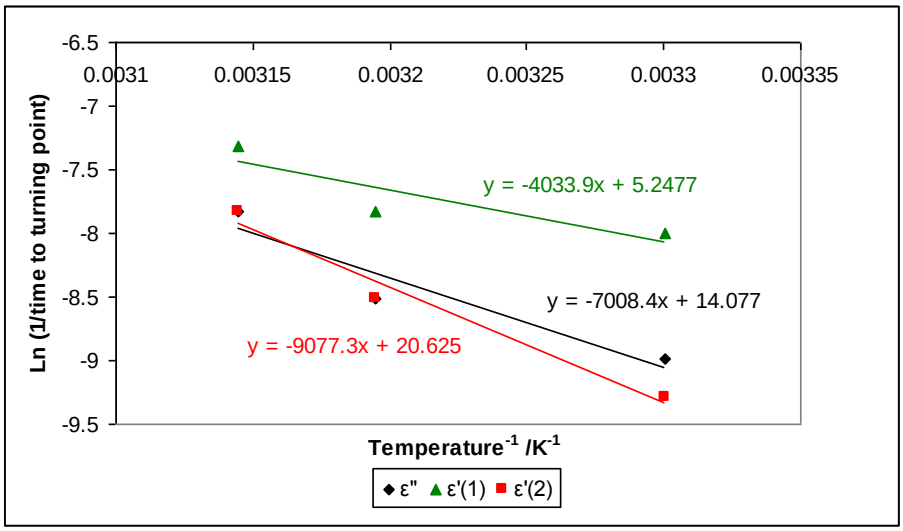


**Figure 7. Arrhenius plot for the Strathclyde model system based on the turning point times calculated from the dielectric data.**

Further discussion of these results and the correlation between the observations from the various techniques will be presented in *Chapter 8*.

## *7.3 SHARED MODEL SYSTEM*

Figure 8 and Figure 9 show the changes in permittivity, plotted against frequency, as a function of cure time for the shared model system at 45°C. Plots for the samples held isothermally at 50°C, 55°C, 60°C and 65°C can be found in the Appendix B (Figures 37-44), and show the same general trends as those observed with the Strathclyde model system. The initial dielectric responses for this system show the characteristic features of heterogeneity reflected in a low frequency relaxation in the ε' plots as a function of frequency (Figure 8). The conduction contribution decreases with time and reflects the increasing viscosity of the media as cure proceeds.

As with the Strathclyde model system, the variation of ε' and ε" were plotted at 2Hz and are shown in Figure 10 and Figure 11 respectively.

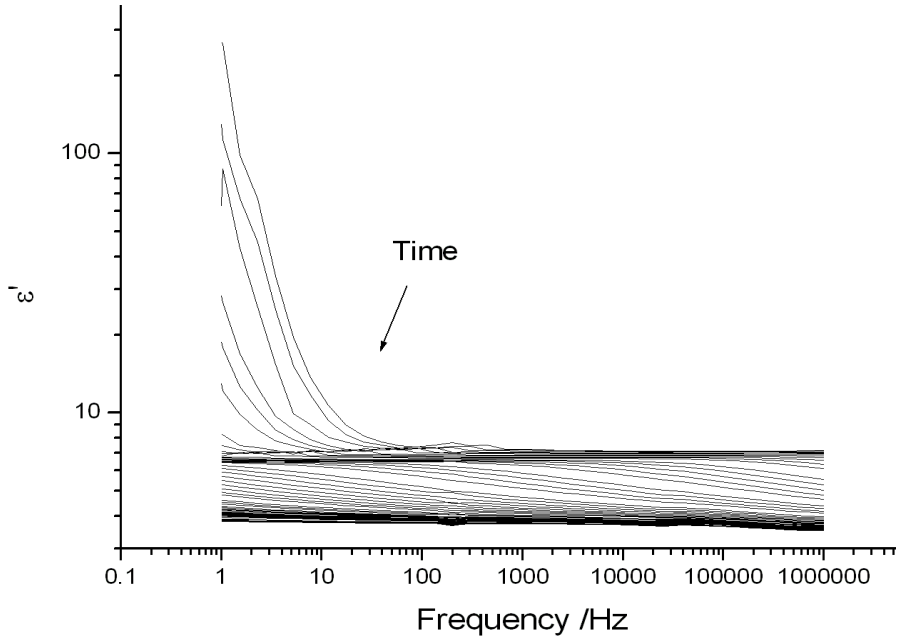


**Figure 8. Plot of real permittivity for the shared model system cured at 45°C as a function of cure time.**

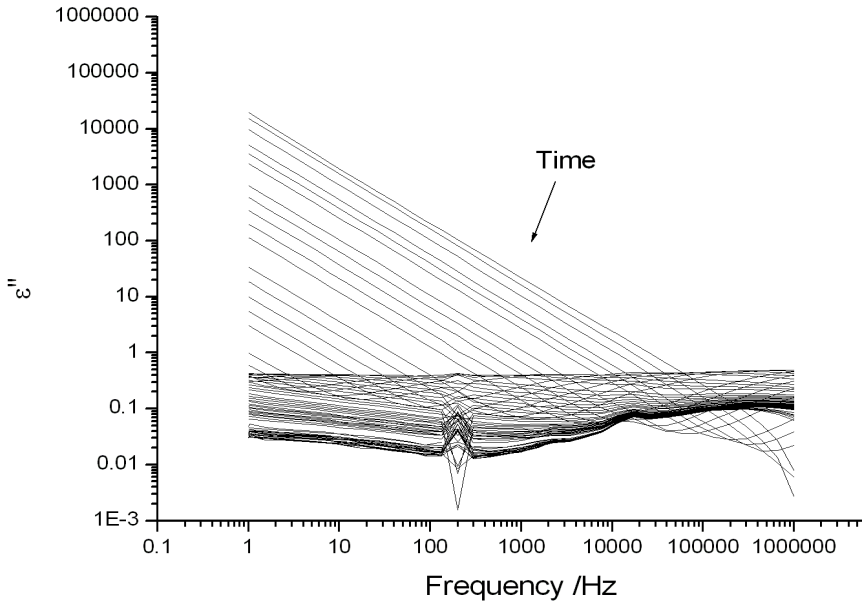


**Figure 9. Plot of imaginary permittivity for the shared model system cured at 45°C as a function of cure time.**

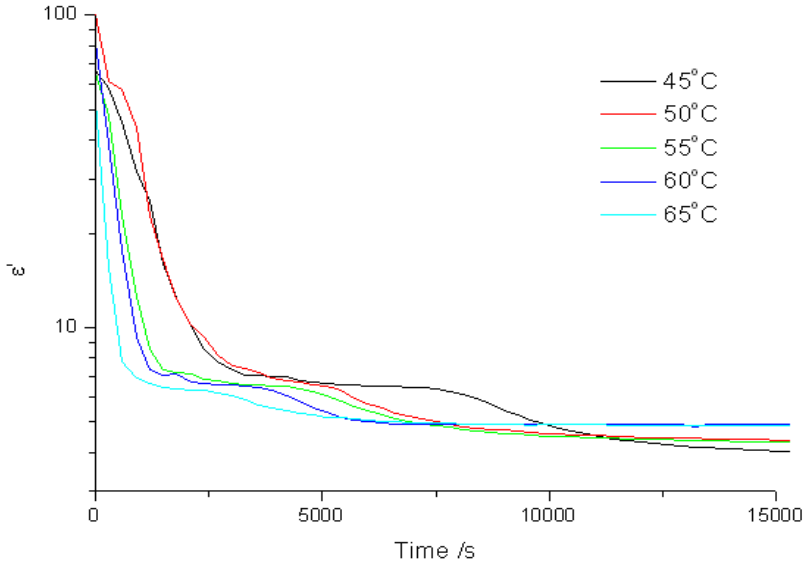


**Figure 10. Plot showing change in real permittivity at 2Hz throughout cure as a function of cure temperature for the shared model system.**

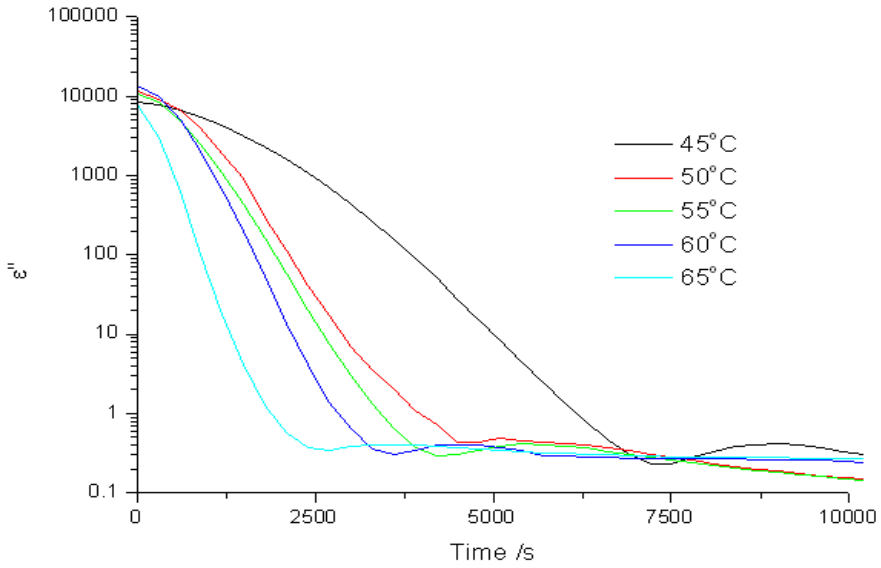


**Figure 11. Plot showing change in imaginary permittivity at 2Hz throughout cure as a function of cure temperature for the shared model system.**

Identification of the turning points for the plots was carried out and the points at which gelation and vitrification occur (in seconds) are included in

Table 2. In this system the loss in the conductivity contribution, as identified by the loss of the 1/ ω contribution, occurs slightly ahead of the feature identified as ε'(2). In all cases the material forms a rigid solid and it is possible to identify the vitrification time, ε'(2).

**Table 2. Turning points for the shared model system (times in seconds).**

| Cure Temperature /°C | ε'(1) /s | ε'(2) /s | ε" /s |
|---|---|---|---|
| 45 | 3125 | 7500 | 7450 |
| 50 | 2900 | 5825 | 4500 |
| 55 | 1650 | 4575 | 4000 |
| 60 | 1250 | 3750 | 3700 |
| 65 | 1200 | 2875 | 2400 |

The activation energy for each of the points of interest was calculated from the Arrhenius plots (Figure 12):

$$E_a\ (\varepsilon'') = 44.0\ \text{kJ mol}^{-1}$$

$$E_a\ (\varepsilon'(1)) = 49.3\ \text{kJ mol}^{-1}$$

$$E_a\ (\varepsilon'(2)) = 42.1\ kJ\ mol^{-1}$$

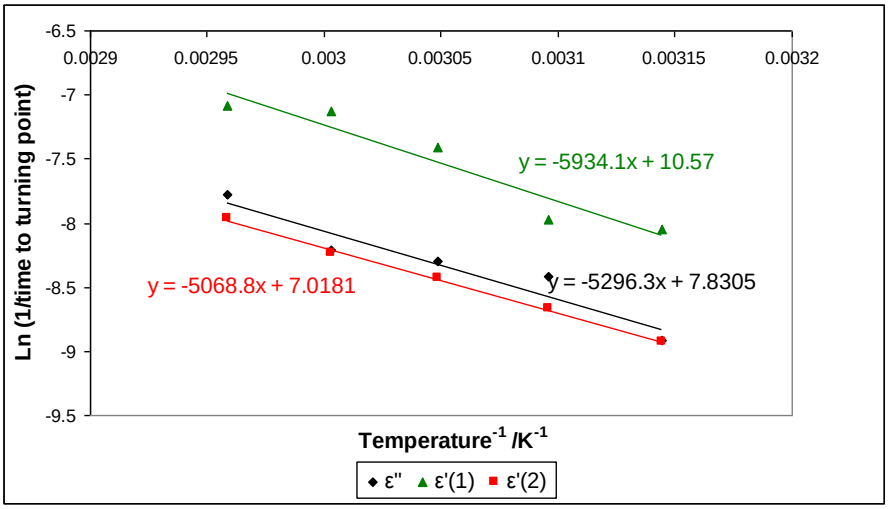


**Figure 12. Arrhenius plot for the shared model system based on the turning point times calculated from the dielectric data.**

Further discussion of these results and the correlation between the observations from the various techniques will be presented in *Chapter 8*.

## *7.4 PR55*

Figure 13 and Figure 14 show the changes in permittivity, plotted against frequency, as a function of cure time for PR55 at 25°C. Plots for the samples held isothermally at 30°C, 35°C, 40°C and 45°C can be found in the Appendix B (Figures 45-52), and show the same general trends. Whilst the times at which the various events change, the overall characteristics of the change in the dielectric spectra with cure time are essentially the same as those observed for the Strathclyde model and shared model systems discussed above.

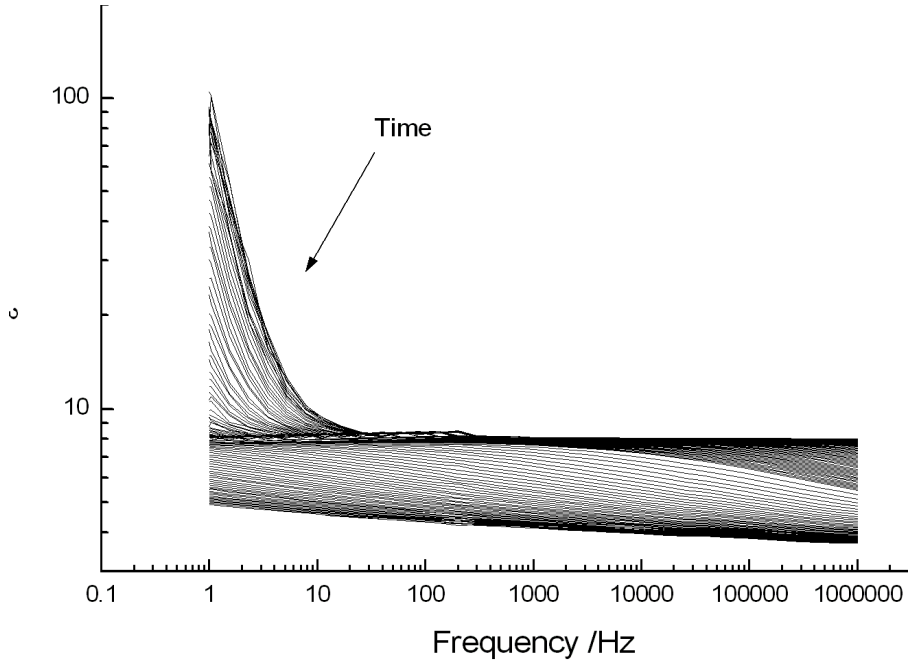


**Figure 13. Plot of real permittivity for PR55 cured at 25°C as a function of cure time.**

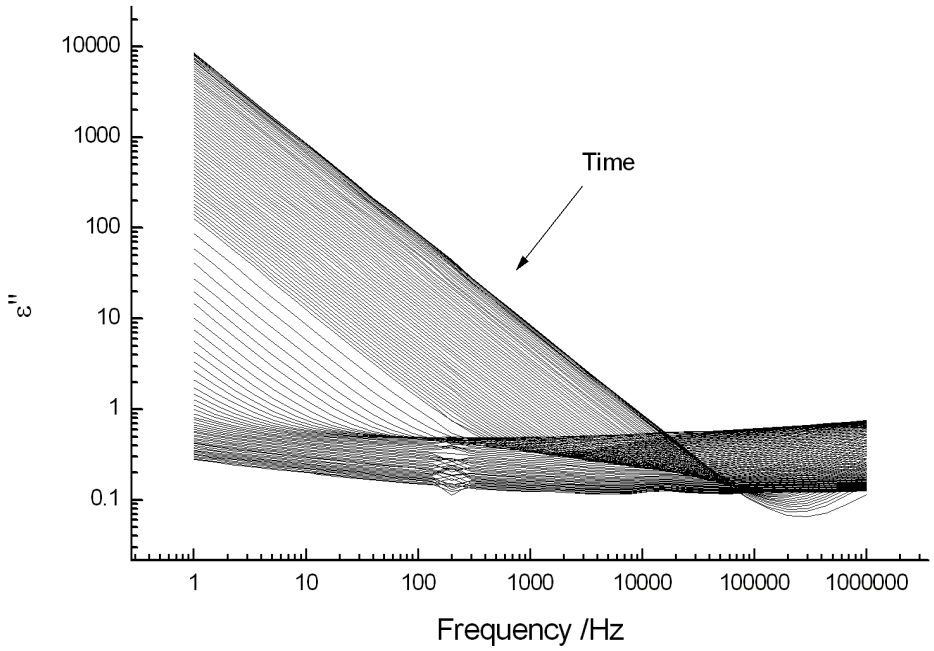


**Figure 14. Plot of imaginary permittivity for PR55 cured at 25°C as a function of cure time.**

The variation of ε' and ε'' were plotted at 2Hz and are shown in Figure 15 and Figure 16 respectively.

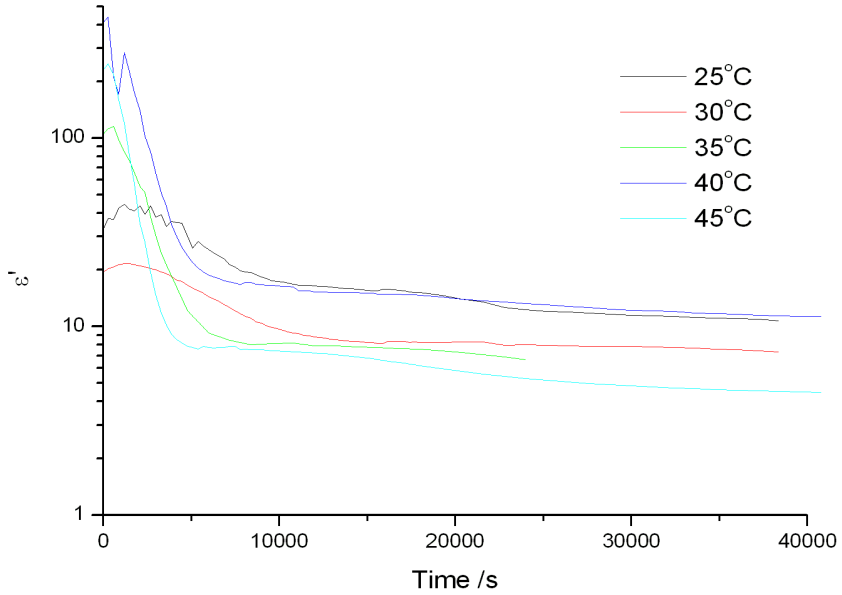


**Figure 15. Plot showing change in real permittivity at 2Hz throughout cure as a function of cure temperature for PR55.**

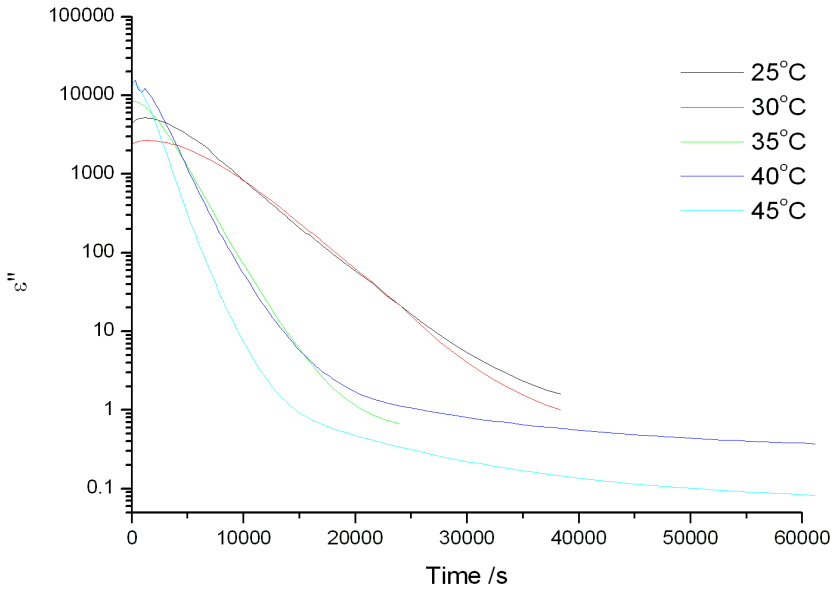


**Figure 16. Plot showing change in imaginary permittivity at 2Hz throughout cure as a function of cure temperature for PR55.**

Analysis of the data provides an estimate of the turning points, given as time in seconds, as indicated in Table 3. At lower temperatures the cure was very slow and as a consequence it is difficult to identify the precise time at which gelation occurs. At the higher temperatures the identification of the turning points becomes easier and more precise values can be quoted.

**Table 3. Turning points for PR55 (times in seconds).**

| Cure Temperature /°C | ε'(1) /s | ε'(2) /s | ε" /s |
|---|---|---|---|
| 25 | 10000 | 23000 | >40000 |
| 30 | 9000 | 23000 | >40000 |
| 35 | 6000 | 21000 | 22000 |
| 40 | 5500 | 19000 | 20000 |
| 45 | 4000 | 15000 | 15000 |

The activation energy for each of the points of interest was calculated from the Arrhenius plots (Figure 17). The first two values for ε" have been excluded as the values for these were not quantified accurately enough. The $E_a$ values were:

$$\mathbf{E_a\ (\varepsilon")} = \mathbf{31.1\ kJ\ mol^{-1}}$$

$$\mathbf{E_a\ (\varepsilon'(1))} = \mathbf{36.6\ kJ\ mol^{-1}}$$

$$\mathbf{E_a\ (\varepsilon'(2))} = \mathbf{16.4\ kJ\ mol^{-1}}$$

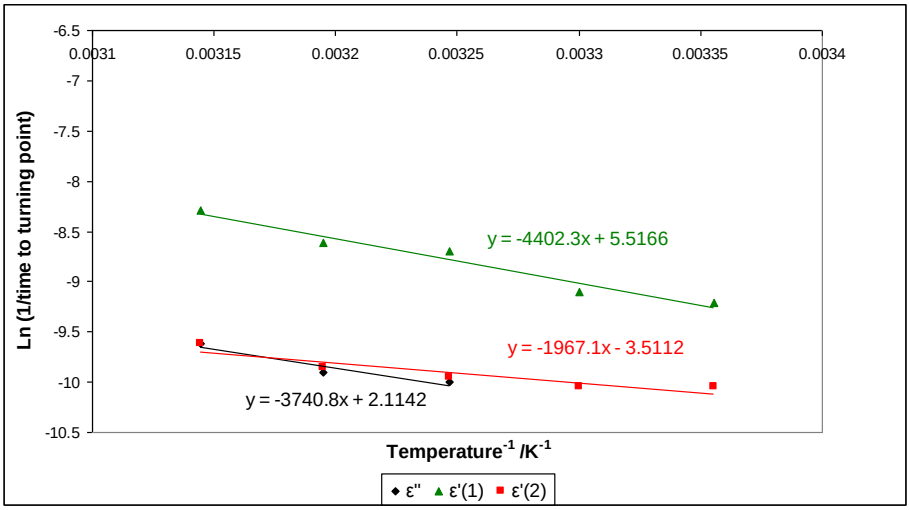


**Figure 17. Arrhenius plot for PR55 based on the turning point times calculated from the dielectric data.**

Further discussion of these results and the correlation between the observations from the various techniques will be presented in *Chapter 8*.

## *7.5 PRIME20*

Figure 18 and Figure 19 show the changes in permittivity, plotted against frequency, as a function of cure time for Prime20 at 40°C. Plots for the samples held isothermally at 50°C, 60°C, 70°C and 80°C can be found in the Appendix B (Figures 53-60), and show the same general trends as previously discussed.

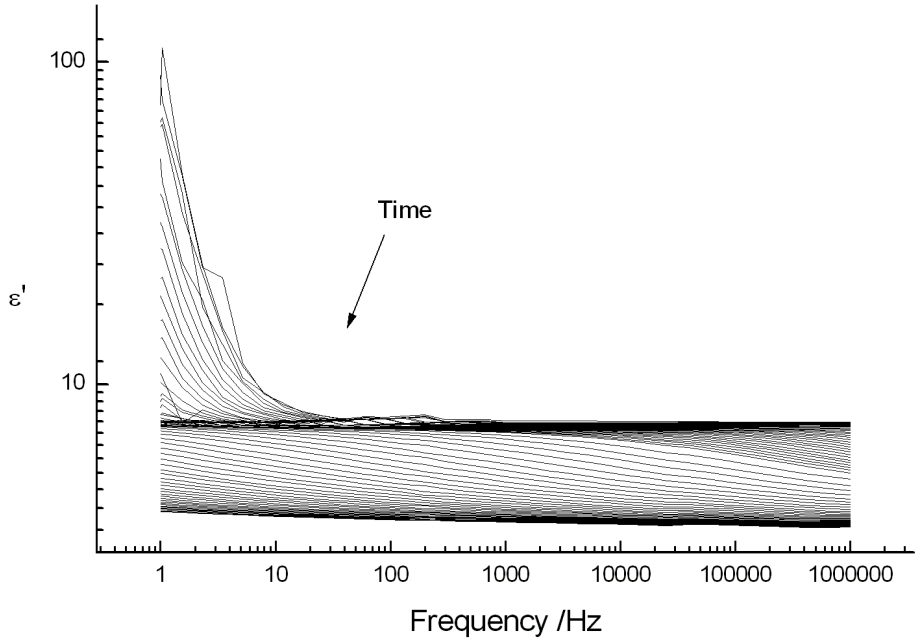


**Figure 18. Plot of real permittivity for Prime20 cured at 40°C as a function of cure time.**

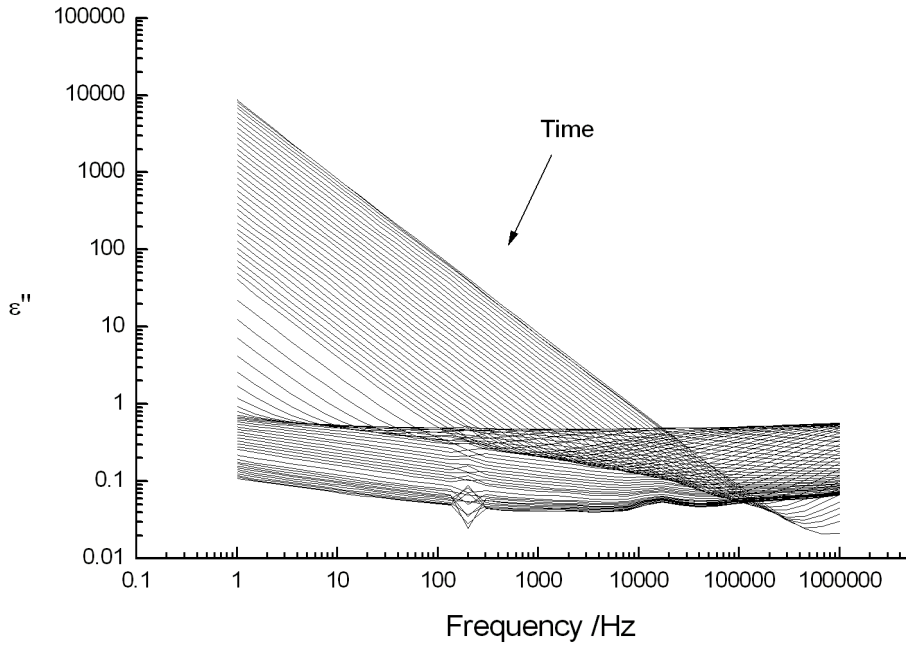


**Figure 19. Plot of imaginary permittivity for Prime20 cured at 40°C as a function of cure time.**

Figure 20 and Figure 21 show the change in the real and imaginary permittivity respectively at 2 Hz throughout cure as a result of the isothermal cure temperature.

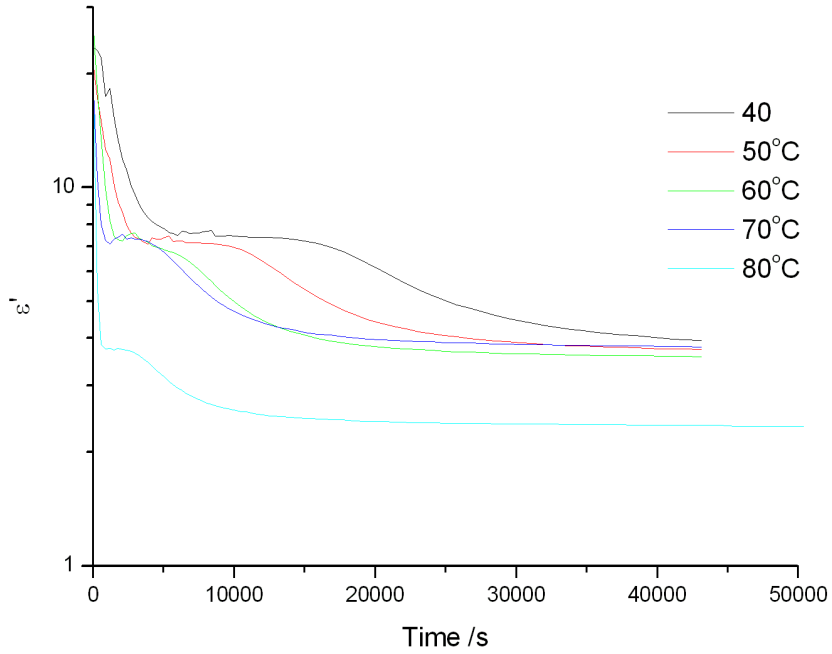


**Figure 20. Plot showing change in real permittivity at 2Hz throughout cure as a function of cure temperature for Prime20.**

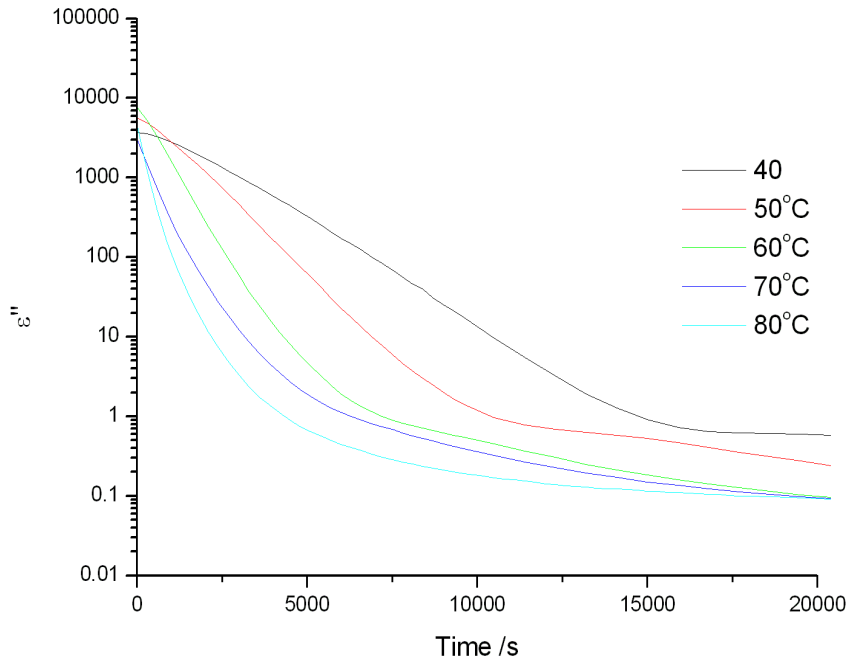


**Figure 21. Plot showing change in imaginary permittivity at 2Hz throughout cure as a function of cure temperature for Prime20.**

Analysis of the data provides an estimate of the turning points, given as time in seconds, as indicated in Table 4.

**Table 4. Turning points for Prime20 (times in seconds).**

| Cure Temperature /°C | ε'(1) /s | ε'(2) /s | ε" /s |
|---|---|---|---|
| 40 | 6000 | 16000 | 15500 |
| 50 | 3000 | 11000 | 10000 |
| 60 | 2050 | 7000 | 7500 |
| 70 | 1500 | 3500 | 6000 |
| 80 | 1000 | 3000 | 4500 |

The activation energy for each of the points of interest was calculated from the Arrhenius plots (Figure 22):

$$E_a\ (\varepsilon'') = 27.5\ \text{kJ mol}^{-1}$$

$$E_a\ (\varepsilon'(1)) = 40.8\ \text{kJ mol}^{-1}$$

$$E_a\ (\varepsilon'(2)) = 41.3\ \text{kJ mol}^{-1}$$

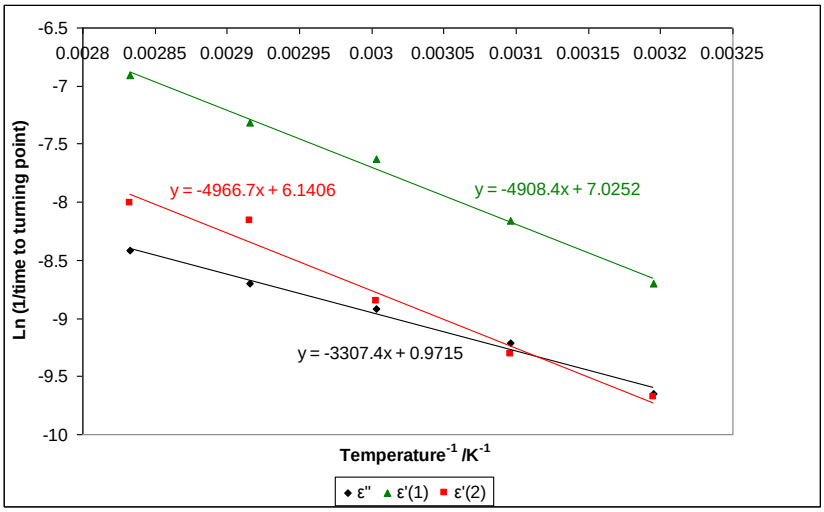


**Figure 22. Arrhenius plot for Prime20 based on the turning point times calculated from the dielectric data.**

Further discussion of these results and the correlation between the observations from the various techniques will be presented in *Chapter 8*.

## *7.6 ADDITIONAL ANALYSIS OF DIELECTRIC SPECTRA*

As indicated in Equation 7.1 and Equation 7.2 it is in principle possible to characterise the dipole relaxation in terms of parameters which are indicative of the strength and distribution of relaxation times for the system. In the initial mixture the dipoles will be associated with the epoxy ring and the amine $NH_2$ and NH functions. As cure proceeds these dipoles will be changed into OH, NH and possibly -O- dipoles. The dielectric process does not differentiate between dipole species but reflects the overall response of the system to the applied field.

Further analysis was carried out on data obtained from a joint study on a model system (LY3505 epoxy resin, which is bisphenol-A/F-based, with XB3403 hardener, a polyoxypropylene diamine), being studied by the group at Birmingham University at 50°C, 60°C and 70°C. The 2D plots at 50°C have been included for reference: Figure 23 and Figure 24.

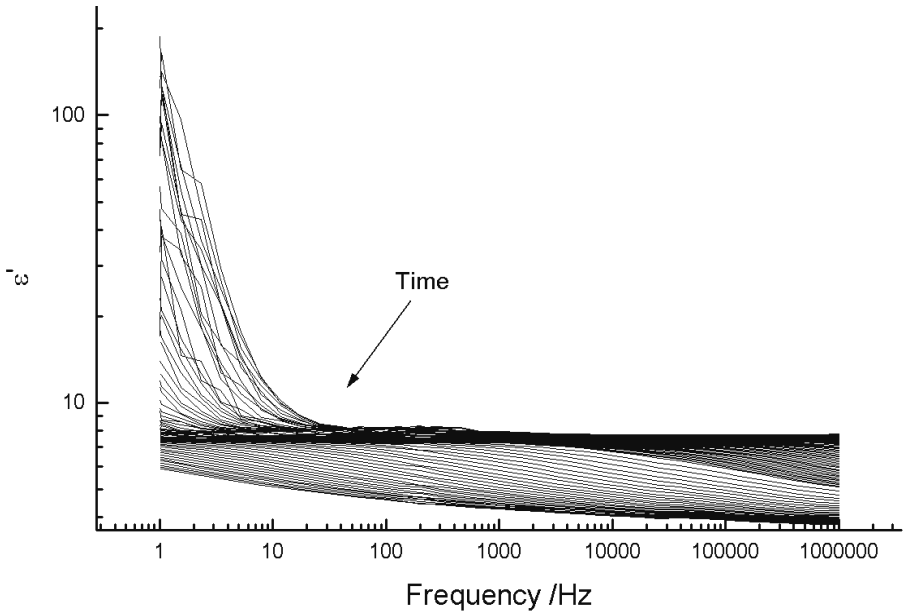


**Figure 23. Plot of real permittivity for the Birmingham model system cured at 50°C as a function of cure time.**

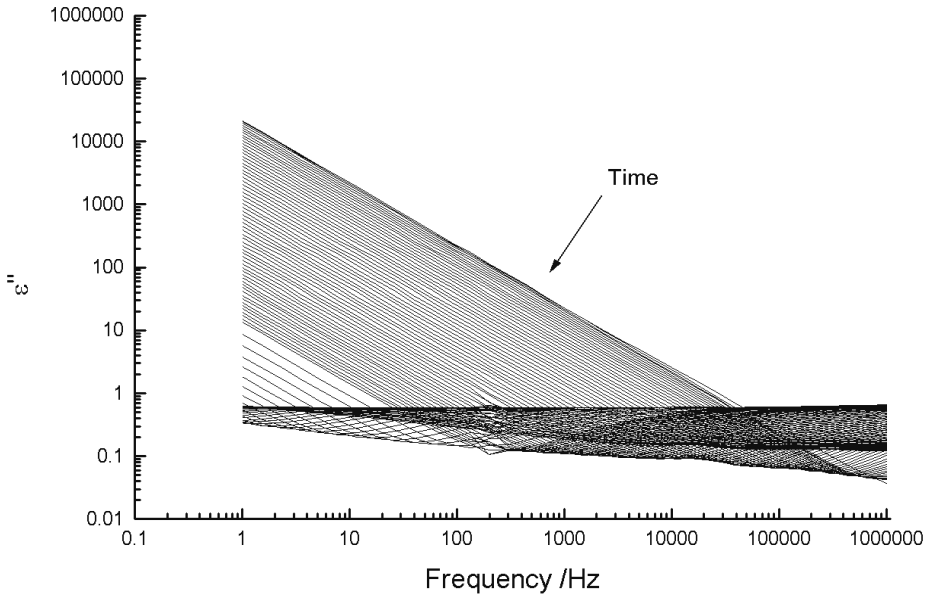


**Figure 24. Plot of real permittivity for the Birmingham model system cured at 50°C as a function of cure time.**

The variation of the values of $\varepsilon'_{\infty}$ are shown in Figure 25. As cure proceeds the value of the $\varepsilon'_{\infty}$ is observed to drop and this is consistent with changes in the packing density of the polymer as the cross linking process occurs. A reduction in the value of $\varepsilon'_{\infty}$ implies that the atom density is reduced and this reflects the restrictions that the cross linking process imposes on the ability for neighbouring chain elements to interact. The point at which the drop occurs coincides with the time at which the system undergoes gelation and vitrification.

The values of the dc conductivity contribution obtained by fitting Equation 7.2 to the imaginary part of the dielectric permittivity are shown in Figure 26. This data parallels that for $\varepsilon''(\omega)$, with the conductivity decreasing as the cure proceeds and the final value reflecting the extent of cure.

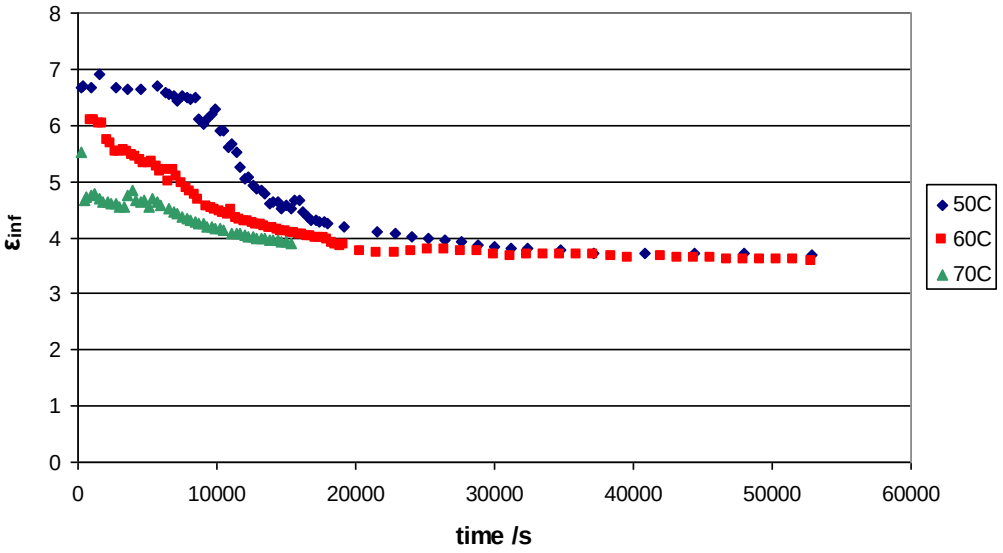


**Figure 25. Variation of the values of ε'$_\infty$ with cure time for the cure of Prime20.**

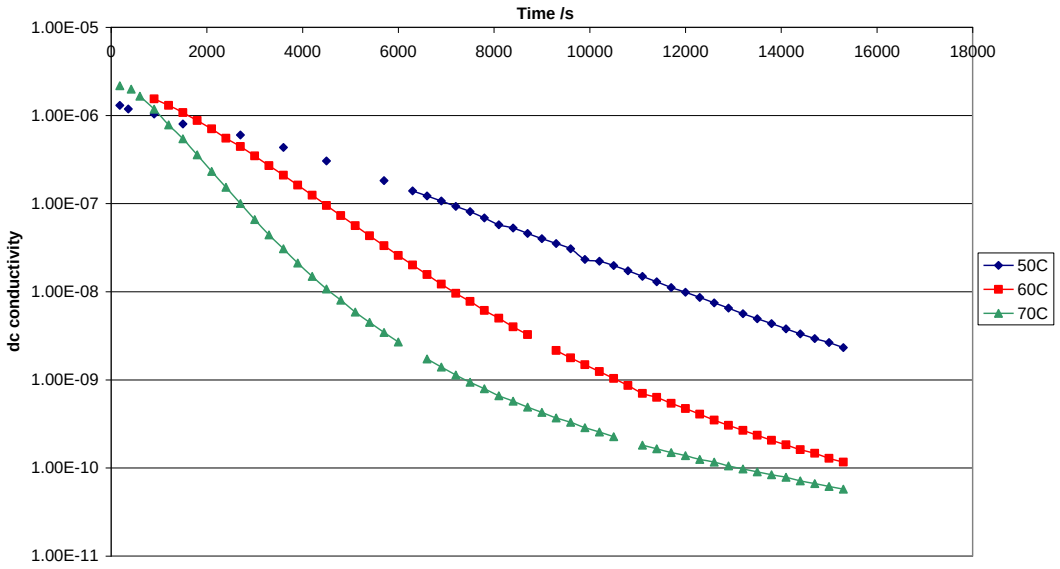


**Figure 26. Variation of the dc conductivity with cure time.**

The relaxation data can be fitted to a single relaxation process and the variation of the fitting parameter α as a function of cure time is shown in Figure 27. The initial low values of the α parameter are a reflection of the data being rather sparse, with the process occurring at high frequency, Figure 28.

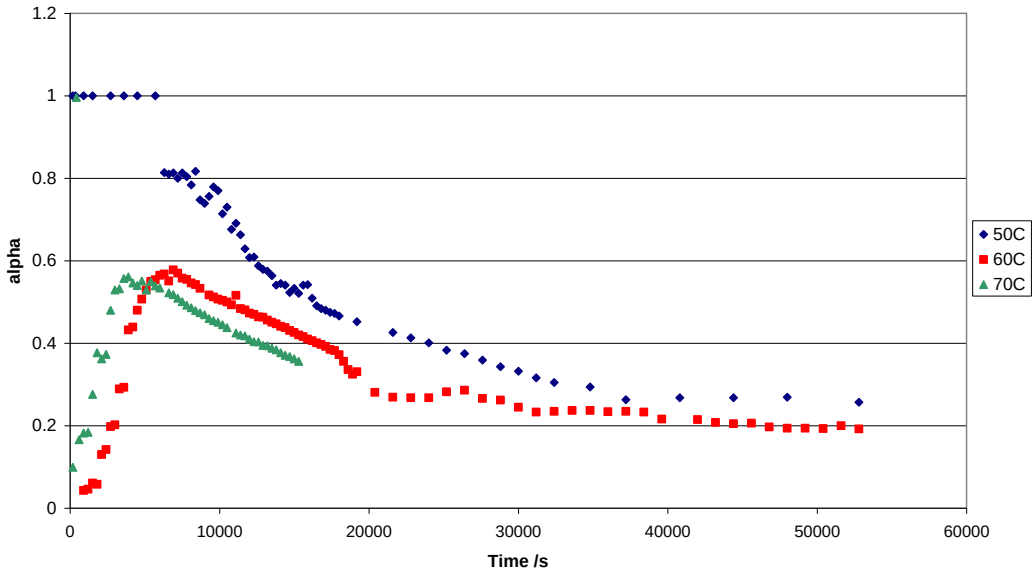


**Figure 27. Variation of the α parameter with cure time.**

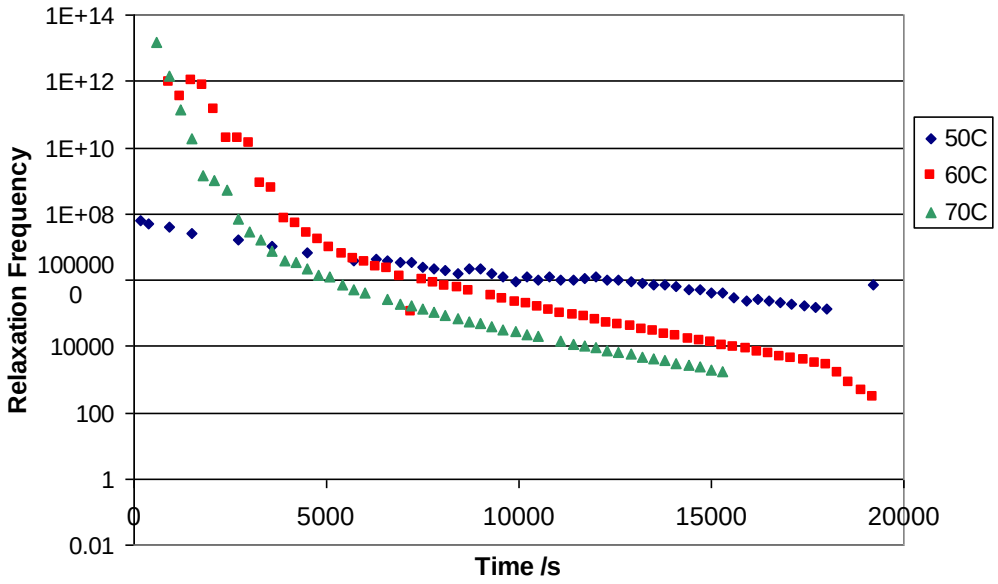


**Figure 28. Variation of the relaxation frequency with cure time.**

The relaxation behaviour is initially that of a low molecular weight liquid and the rate of rotation of the dipole is controlled by the viscosity of the fluid. As the viscosity increases, so the rate of rotation will decrease as reflected by the decrease in the value of relaxation frequency as the cure time increases. However, as cure proceeds the dipole changes from that of a single dipole attached to a monomer to a pendant OH dipole with the motion being influenced by the whole molecular motion

of the polymer and its reorientation as a pendant group to the polymer chain. As the molecular weight increases so the whole molecule rotation will make a decreasing contribution to the dipole relaxation and the process will be influenced by the environment around the pendant OH group. As the matrix changes from a gel to a rigid solid so the interactions will increase and this will lead to the process dropping to lower frequency.

The variation of the amplitude of the relaxation process, Δε, as the cure proceeds, is illustrated in Figure 29. The amplitude of the process is initially fairly constant reflecting the dominance of small molecule rotation in the initial stages. Depending on the rate of cure so the point at which the magnitude of the Δε increment increases changes with time. The increment increasing steadily with time reflects the increasing concentration of OH dipoles as the epoxy rings are opened. The slight decrease in the amplitude of the Δε increment at long times is consistent with some of the OH groups being consumed in the autocatalytic ether formation.

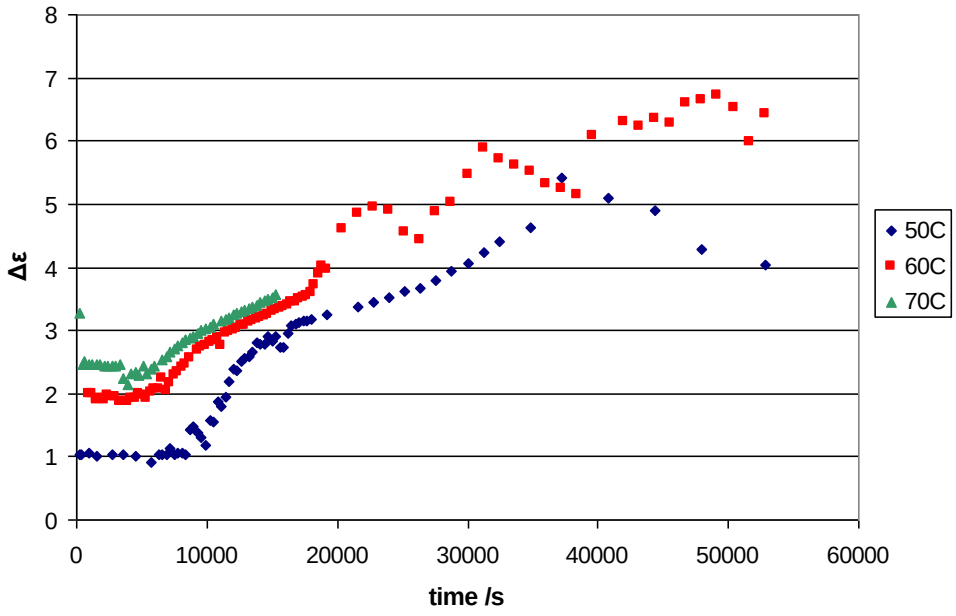


**Figure 29. Variation of the amplitude of the relaxation process as a function of cure time.**

The dielectric data presented indicate the way in which, as the cure process proceeds, the dipole relaxation change is consistent with the change in the nature of the dipole and also the effects of the increase in the molecular weight and restrictions imposed

by gelation on the relaxation process. The results of the joint work with Birmingham University have been included for illustrative purposes however the other systems considered within this thesis were not further analysed using this approach.

## *7.7 CONCLUSIONS*

Despite the significant differences in the chemistry taking place during the cure process the dielectric changes are all very similar across the systems studied and allow identification of the critical points associated with the gelation and vitrification of the material. The data obtained will be compared with those obtained from the other techniques in *Chapter 8*.